



Numerical and Experimental Study of Abrupt Wave Interaction with Vertical and Inclined Rectangular Obstacles

R. Memarzadeh^{1†}, H. Sheybanifard² and M. Zounemat-Kermani³

¹ *Department of Civil Engineering, Faculty of Engineering, Vali-e-Asr University of Rafsanjan, Rafsanjan, Iran*

² *Department of Water Engineering, Faculty of Water and Soil, Gorgan University of Agricultural Sciences & Natural Resources, Gorgan, Iran*

³ *Department of Water Engineering, Faculty of Agricultural Engineering, Shahid Bahonar University of Kerman, Kerman, Iran*

†*Corresponding Author Email: r.memarzadeh@vru.ac.ir*

(Received June 13, 2020; accepted November 5, 2020)

ABSTRACT

The aim of the present paper is the study of interaction of the abrupt wave with vertical and inclined rectangular obstacles. For this purpose, in the first step, two experiments have been done. The tests were performed with smooth rectangular cross-section channels, and related data were extracted using digital image processing. Flow behavior was recorded with one adjacent CCD camera through the glass walls of the entire downstream channel. In the second step, the numerical study has been done by a mesh-free particle Lagrangian method (Incompressible Smoothed Particle Hydrodynamics, ISPH) and a mesh-based Eulerian method (Finite Volume Method with Volume of Fluid surface tracking approach, FV-VOF). The capabilities of the numerical methods in simulation of the sudden variations free surface flows have been assessed. A comparison between the computed results and the experimental data shows that both numerical models simulate the mentioned flows with reasonable accuracy.

Keywords: Free-surface flows; Abrupt wave; Fluid-solid Interaction; Experimental modeling; Numerical modeling; ISPH; FVM.

1. INTRODUCTION

Abrupt wave such as the dam break flow has a potential flood hazard. Therefore, it is essential to correctly simulate abrupt waves to diminish the potential damages of a potentially disastrous flood e.g. due to a dam break or breach of a dam. The simulation process can be done by either physical or numerical models (Ozmen-Cagatay *et al.* 2014; Zhang *et al.* 2018). In the previous studies, different researchers have studied the flow interaction with the obstacles (e.g. Soares-Frãzao and Zech, 2007; Bukreev, 2009; Aureli *et al.* 2015). Since establishing physical models for real-world cases is a time-consuming and expensive process, robust numerical models are suitable alternatives for flow simulation.

As the main focus of this paper is the use of two numerical approaches, including mesh-less SPH Lagrangian and mesh-based FV-VOF Eulerian

methods for study the topic of present paper. Related studies are mentioned below. SPH, a versatile and powerful numerical method, is based on a Lagrangian approach and has been successfully applied to many industrial, mechanical, and environmental fluid flows (Memarzadeh and Hejazi, 2012; Chen *et al.* 2015; López *et al.* 2018; Hosseinkhani *et al.* 2020; Kheirkhahan *et al.* 2020). In SPH method, the computational domain is represented by a set of particles where physical quantities such as pressure, density, velocity and position are known. These particles move with the fluid in a Lagrangian coordinate, and their properties change with time because of the interactions with neighboring particles (Shao and Lo, 2003).

Apart from its usage in the simulation of elasticity and fragmentation in solids, SPH has been utilized to simulate the interaction between fluid-solid and different fluids. Crespo *et al.* (2008) demonstrated that using a 2D version of the SPH model can be

considered as a suitable tool to reproduce a dam-break evolution over dry and wet beds. Also, their developed model makes possible the study of different propagation regimes during the dam-break evolution. [Khayer *et al.* \(2018\)](#) used an enhanced ISPH method to simulate wave interactions with a porous medium. The computational results of this study demonstrated that the ISPH flow model could be a promising simulation tool in coastal hydrodynamic applications. [Canelas *et al.* \(2016\)](#) developed the hybrid SPH–DCDEM model for free surface solid–fluid flows. The model results show that SPH–DCDEM model is capable of treating highly complex interactions, such as hydrodynamic actions on structures. [Canelas *et al.* \(2018\)](#) used the DualSPHysics model to study the fluid–structure–structure interaction flows. [Chang *et al.* \(2011\)](#) proposed the SPH model to investigate shallow-water dam-break flows in 1D open channel. The simulated results indicated that the proposed model could perform well even in the presence of shock discontinuities and in conditions with abrupt pressure gradients such as shock front motion and hydraulic jumps. [Xu *et al.* \(2013\)](#) present an improved SPH method and its interesting extension to 3D non-Newtonian free surface flows, which are modeled by the Cross model. [Memarzadeh *et al.* \(2018\)](#) applied a mesh free Lagrangian two-dimensional non-cohesive sediment transport model based on the SPH method to a two-phase flow over an initially trapezoidal-shaped sediment embankment. Furthermore, the SPH method has been successfully used to simulate the interaction of fluid flow and rigid bodies. [Marrone *et al.* \(2011\)](#) developed a SPH model with numerical diffusive terms for the prediction of loads of impact flows on solid structures with arbitrary shapes. [Hui Pu *et al.* \(2013\)](#) simulated dam-break flows in the presence of a triangular hump using two models; SGUM-SWEs model and ISPH model. [Albano *et al.* \(2016\)](#) a 3D SPH model to the design of flood mitigation measures. In their study, first the developed model validated using simulation of a dam breach that strikes two fixed obstacles and three transportable floating bodies. Then, the validated SPH model has been used to examine different configurations to identify the best layout for urban area flash-flood damage mitigation.

In addition to the SPH technique in simulating free-surface fluid flow interactions, solving governing equations in an Eulerian approach with the FV method, and the aid of the concept of volume of fluid approach (FV-VOF) has received considerable attention. [Mokarni and Abadie \(2016\)](#) addressed the problem of numerical simulation of dynamic loads generated during a dry dam-break flow impact on a wall. The numerical model used was a multi-fluid Navier–Stokes FV-VOF model. They found that the computed pressure peaks behave differently depending on the distance to the stagnation point of free-slip boundary conditions of the wall. [Tang *et al.* \(2016\)](#) applied an overlapping moving-particle semi-implicit (MPS) method as well as the FV-VOF model for a 3D dam-break free surface flow. The qualitative comparison among experimental data and the results obtained by FV-VOF and MPS

showed that the shape of the free surface obtained by the overlapping MPS is more accurate than that of FV-VOF.

Simulation of an abrupt wave flow is a challenging process for numerical models, especially with an obstacle in the channel. In the previous studies, the interaction of abrupt waves with inclined obstacles has not investigated. Moreover, the evaluation of numerical models with the mentioned test shows their ability to accurately simulate complex free surface problems. This paper aims (i) to carry out experimental study of abrupt waves including a dam-break flood wave and sudden release of flow under a sluice gate facing vertical and inclined obstacles in initially dry flumes, and (ii) to investigate the performance of ISPH and FV-VOF methods in simulating the complex behavior of free surface waves. In the experimental tests, rectangular-shaped bottom obstacles (vertical and inclined) were placed downstream of the barrier (representing the dam) and sluice gate to provide the effects of obstacles on the propagation of flood waves. Simultaneously, two sets of numerical model tests were performed by ISPH Lagrangian mesh-free numerical method as well as Eulerian mesh-based numerical method based on the FV-VOF approach with setup and boundary conditions identical to the experimental models.

The paper is organized as follows: In section 2, the experimental setups and description of physical models are described. In section 3, the governing equations of the phenomena are mentioned, and numerical formulations are expressed. The results of experimental and numerical models are provided in section 4, as well as the assessment of the accuracy of numerical models. In this section, the discussion about the numerical findings is provided. Finally, the major conclusions of the study are stated in the section 5.

2. EXPERIMENTAL SETUPS AND DESCRIPTION OF PHYSICAL MODELS

The experiments been carried out by the authors in the Water Engineering Laboratory of the Shahid Bahonar University of Kerman, Iran. Figure 1 shows the sketch of experimental models, and their main dimensions. The tests were performed in a 1 m long, 0.5 m deep and 0.5 m wide flume. The walls of the flume were made of glass with roughness height equal to 0.003 mm. Both of the obstacles in Test A and Test B have a length of 0.1 m and a width of 0.01 m. the obstacles occupy the entire width of the flume. In the first experiment, the obstacle is placed vertically and in the second experiment, the obstacle is placed at an angle of 60 degrees to the horizon.

A sluice gate was placed at about half of the flume length. The water stored in the reservoir at behind of the gate. In Test A, dam break wave interaction with the vertical obstacle was took place with suddenly moving up of the gate. In Test B, the gate was opened 5 cm, and the water flow propagated

over the downstream reach, which hit the inclined obstacle. In order to ensure the correct movement of the gate, the gate displacement is repeated several times before each test. What are presented as the results of two experimental tests are their best results.

The coordinate system used to present the data has the x-axis and z-axis originates at the bottom of the flume (Fig. 1).

Measurements were obtained using image analysis. A video-camera positioned at one meter the lateral side of the channel recorded the evolution of the flow propagation. The relation between image pixels and space coordinates was obtained via a reference grid glued to the lateral side of the channel. The camera had a resolution of 5184 × 3456 (18.0 effective megapixels) at 21.7-bit color depth. The longitudinal profiles of the abrupt wave flow were extracted from the images after basic pre-processing by manual digitalization. In this process, the images are coordinated by considering several points that have specific coordinates in the laboratory flume, and the exact characteristics of the flow profile are extracted for later use.

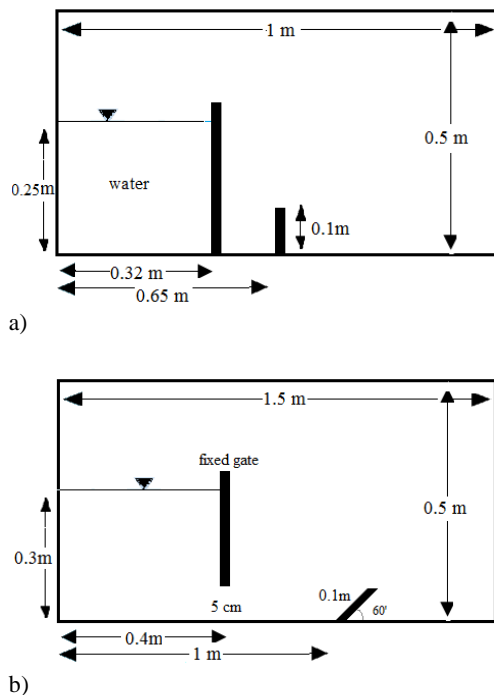


Fig. 1. Schematic sketch of the experimental setup in Test A and Test B.

3. NUMERICAL MODELING

3.1. Governing Equations

The governing equations of wave flow are only mass conservation (1) and momentum conservation (2) equations (Navier-Stokes, 2D vertical), as follows (Monaghan, 2000):

$$\frac{1}{\rho} \frac{D\rho}{Dt} + (\nabla \cdot \mathbf{u}) = 0 \quad (1)$$

$$\frac{D\mathbf{u}}{Dt} = -\frac{1}{\rho} \nabla P + \frac{\mu}{\rho} (\nabla^2 \mathbf{u}) + \mathbf{g} \quad (2)$$

In the above equations, $D\mathbf{u}/Dt$ the full derivation of time, ρ is density, \mathbf{u} is the velocity vector, μ denotes the dynamic viscosity, P is pressure, \mathbf{g} is the gravitational acceleration, and t is time. On the right side of Eq. 2, the first term indicates the pressure gradient, the second term the effects of fluid viscosity, and the third term is the gravitational acceleration (\mathbf{g}).

3.2. Numerical Solution Algorithms

3.2.1. ISPH Formulation and Solving Algorithm

The SPH method is based on integral interpolation for approximation equations (Monaghan, 2000):

$$f(\mathbf{r}_i) = \sum_{j=1}^n \frac{m_j}{\rho_j} f(\mathbf{r}_j) \hat{W}(|\mathbf{r}_i - \mathbf{r}_j|, h) \quad (3)$$

Where m_j and ρ_j are the mass and density of particle j , \hat{W} is the smoothing function, \mathbf{r} is position vector, h is smoothing distance. Discretization of pressure and viscosity terms in Navier-Stokes (NS) equations by the SPH method is as follows (Memarzadeh *et al.* 2018):

$$\frac{1}{\rho_i} (\nabla P_i) = \sum_j m_j \left(\frac{P_j}{\rho_j^2} + \frac{P_i}{\rho_i^2} \right) \cdot \nabla_i \hat{W}_{ij} \quad (4)$$

$$\left(\frac{\mu}{\rho} \nabla^2 \mathbf{u} \right)_i = \sum_j \frac{2m_j \left(\frac{\mu_i}{\rho_i} + \frac{\mu_j}{\rho_j} \right) \mathbf{r}_{ij} \cdot \nabla_i \hat{W}_{ij}}{(\rho_i + \rho_j) (|\mathbf{r}_{ij}|^2 + \eta^2)} (\mathbf{u}_i - \mathbf{u}_j) \quad (5)$$

Where $\mathbf{r}_{ij} = \mathbf{r}_i - \mathbf{r}_j$ and $\eta = 0.01 \times dr$ is a small number which is introduced to keep the denominator no-zero during computation.

In the present study, the authors developed an ISPH model with a two-step fractional algorithm to solve the governing equations. In the first step, Navier-Stokes equations are solved to compute velocity components by omitting pressure terms. In the next step (correction step), the pressure force is used to correct the particle velocities. The pressure is calculated from the Poisson equation (Shao, 2010).

For modeling the solid walls, they are treated by fixed wall particles. The velocities of wall particles are set to zero to represent the non-slip boundary condition. Furthermore, the particle density is used to determine the free surface, and a zero pressure is assigned to the free surface particles. If the particle density is less than 97% of the water density, it is identified as a free surface particle (Shao, 2010).

3.2.2. FV Formulation with VOF Free-Surface Technique

The FV method is mainly based on the Eulerian approach, and it is known as a comprehensive and common technique in CFD problems. In this method, the computational domain is divided into a limited number of cells that together form a network on which the governing differential equations are resolved. Detailed information about FVM can be found in many related resources (Versteeg and Malalasekera, 2007).

In this paper, simulation of abrupt wave interaction with solid bodies with FV-VOF method was performed using a commercially available computer fluid dynamics model, Ansys/Fluid flow (CFX) v.16 software, which solves the Reynolds-Averaged Navier–Stokes (RANS) equations. The equations were discretized using the FV method. For displacement of the free surface, the VOF method was adopted with a local height function. The high resolution numerical scheme was used for discretizing the advection terms. The standard $K-\epsilon$ turbulent model was used in CFX. Ansys CFX uses a coupled technique to link the pressure/mass equation to the momentum equation where the pressure/mass equation is solved simultaneously with the momentum equations in one big matrix. This requires more memory to solve, but for most cases converges far faster.

4. RESULTS

4.1. Experimental Results

Immediately after opening the gate, the abrupt wave propagated, hit the obstacle, and with high turbulence flowed on the downstream. Subsequently, the progressive wave interacted with the right-hand side wall of the flume, and moved upward. Furthermore, secondary waves derived from the reflections of the traveling wave between the left-hand side of the flume wall and obstacle, with a progressive attenuation.

The above described abrupt wave dynamics for the two tests, including vertical and inclined obstacle is supported by the temporal evolution of the free surface profiles shown in Fig. 2 and Fig. 3. In the mentioned Figures, the flow appears by the color region. The observed front of the wave represents a fast propagation of water waves. Although the general characteristics time scale of both tests is similar, the behavior of the free surface temporal variation is very different.

4.2. Application and Evaluation of Numerical Models

As described in the previous section, the interaction between abrupt wave and solid obstacle results in a free surface flow with high varied free surfaces. To assess the performance of the above-mentioned models i.e., ISPH and FV-VOF models in reproducing the performed experiments, the longitudinal free-surface profiles have been compared to the corresponding measured ones.

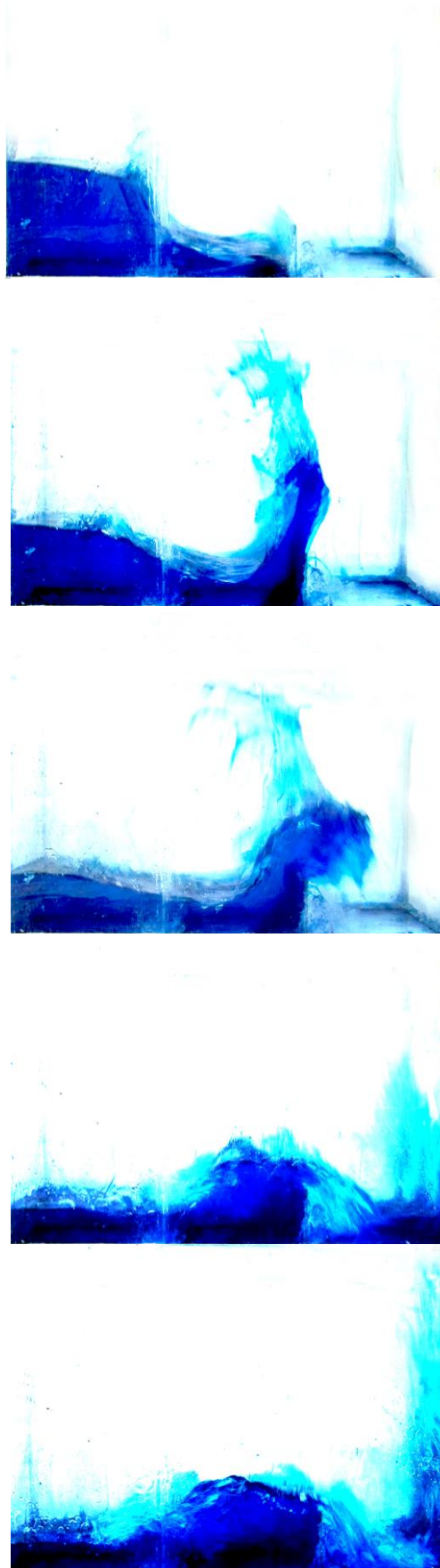


Fig. 2. Snapshots of laboratory photographs for the abrupt wave collision with the vertical obstacle at times 0.2, 0.4, 0.6, 0.8 s and 1 s.

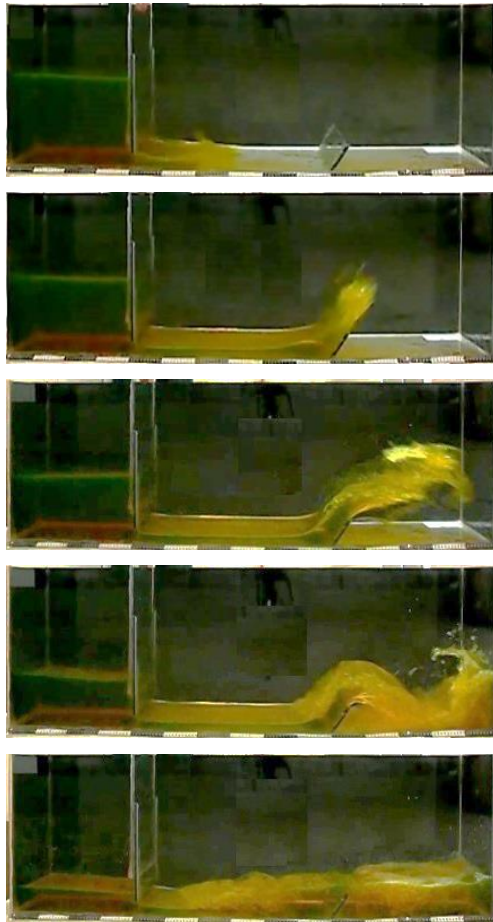


Fig. 3. Snapshots of laboratory photographs for the abrupt wave collision with the inclined obstacle at times 0.2, 0.4, 0.6, 0.8 and 1.0 s.

4.2.1. Numerical Modeling of Abrupt Wave Impact with a Vertical Obstacle

The first analysis is performed by simulation of the abrupt wave caused by sudden dam removal and the hydrodynamic impacts on the vertical obstacle. A schematic view of the discretized physical domain in FVM and initial location of particles in ISPH methods, are shown in Fig. 4. The structured rectangular grids have been used to discretize the computational domain. The grids are applied perpendicular to each other to minimize the interpolation error between them.

Before each simulation, the convergence study has been performed for both models. The main purpose of the convergence study is finding the best mesh or particle size for the simulation with low computational cost. Here, one of these studies is presented. The convergence study of FV-VOF model has been performed with different total number of meshes including 6359, 9376, and 13045. Furthermore, The ISPH simulations have been done with three particle sizes of 0.006, 0.004, and 0.002 m. In Fig. 5 and Fig. 6, the quantified comparison of the models' results with different mesh or particle resolution and experimental data are presented. These Figures show that the accuracies of models improve when the numbers of

meshes or particles are increase. Since the computational time with the largest number of meshes or particles is significantly different from the computational time with the average numbers of meshes or particles, and the accuracy of the simulations has not increased much, so it can be said that the models have been converged. In the following, the simulations are performed with the average size of meshes or particles.

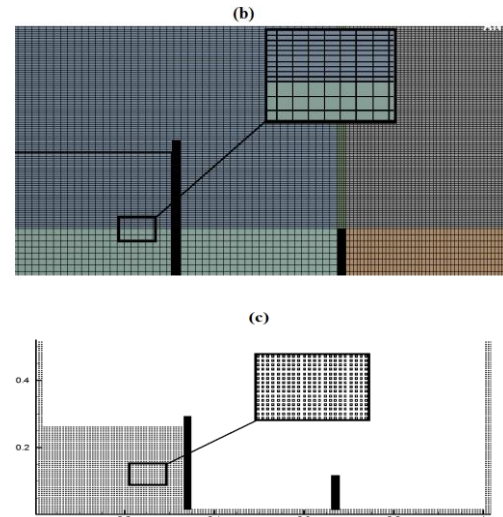


Fig. 4. b) Schematic view of numerical rectangular meshes in the FV-VOF approach, c) Schematic view of initial location of the particles in the ISPH approach at the initial time.

The results of the models with median numbers of meshes of particles are illustrated and compared with experimental depictions in Fig. 7. The primary wave is accurately tracked in pre-collision times. The secondary wave, which is formed after the flow strikes the obstacle, mounts on the base flow, and it moves upwards. As can be seen from the Fig. 7, the primary wave is present as the main current for up to 0.8 seconds. Then, in 0.8 seconds, the current moves upward and interferes with the downstream flow, which is relatively slow. At this point, a large part of the kinetic energy of the current is dispersed due to the energy dissipation vortices. What is clear from Fig. 7 is that both numerical models perform reasonably well in predicting flow characteristics before and after the flow strikes the obstacle and forms a secondary wave. For a better understanding and more comprehensive analysis of the results, the free surface profiles and the positions of wave front as a function of dimensionless time obtained numerically and experimentally are given in Fig. 8 and Fig. 9, respectively.

According to Figs. 8 and 9, the free-surface profiles obtained by both FV-VOF and ISPH methods are in good agreement with experimental observations. In order to evaluate the numerical models, statistical criteria including mean absolute error (MAE, Eq. 6) is used. The MAE factor expresses the mean error between numerical model and experimental data,

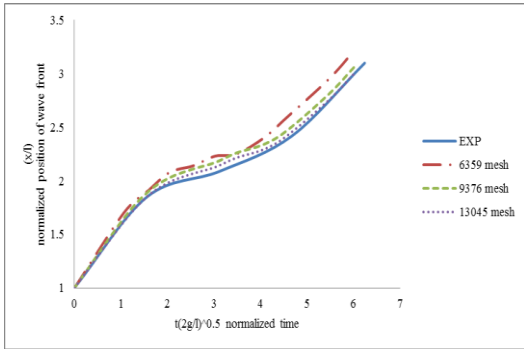


Fig. 5. Comparison of the present model results with different total number of meshes with the experimental data.

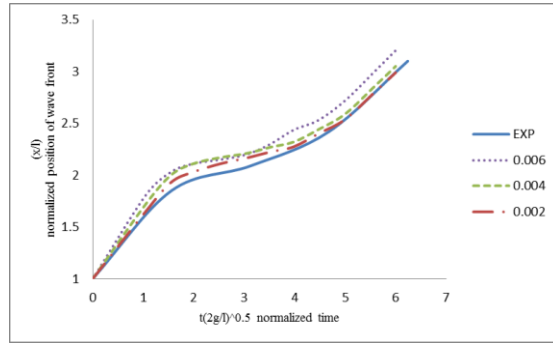


Fig. 6. Comparison of the present model results with different initial particle spacing with the experimental data.

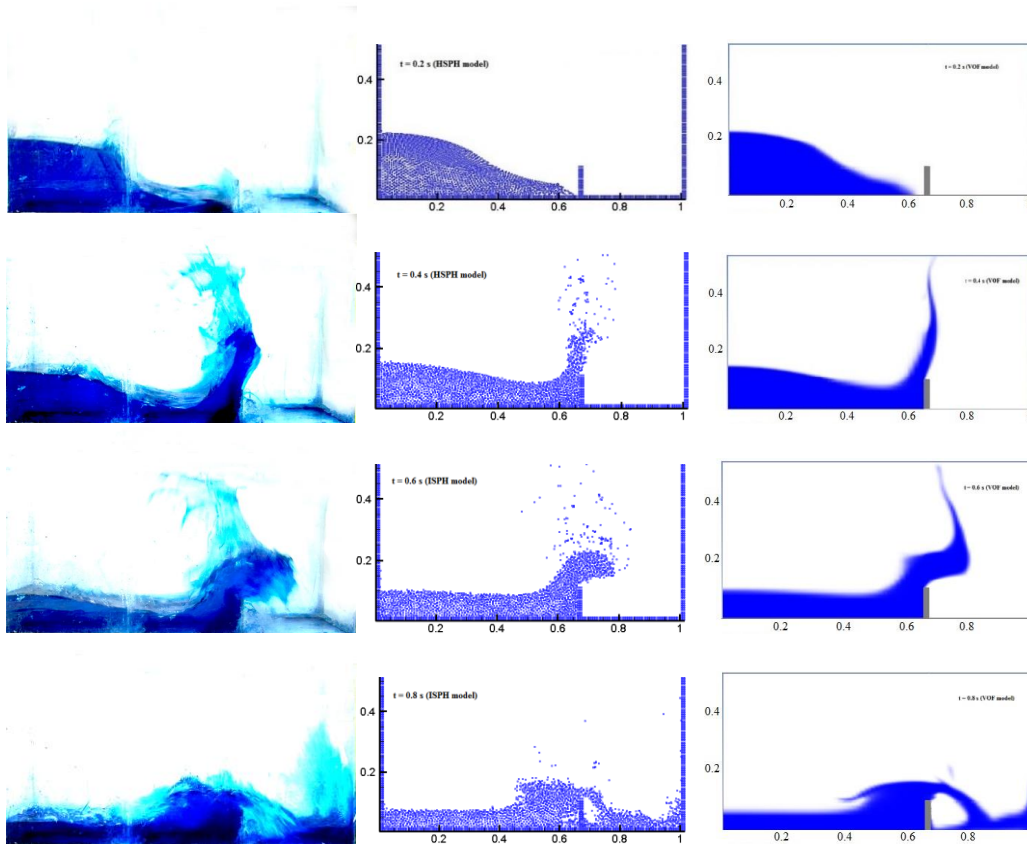


Fig. 7. Snapshots of computational results (FV-VOF on the right and ISPH in the middle) and laboratory photographs (on the left) at times 0.2, 0.4, 0.6, and 0.8 s.

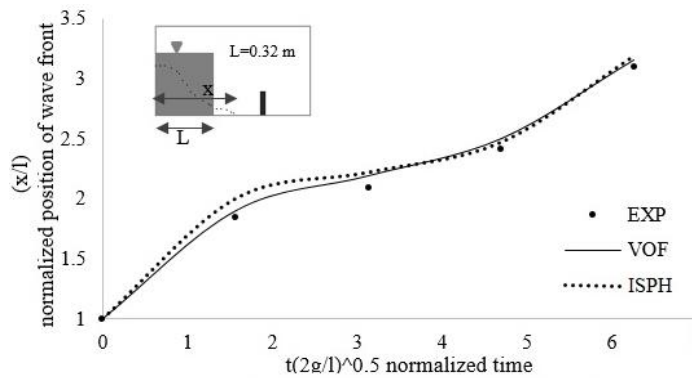


Fig. 8. Experimental versus numerical normalized diagram of wave front position for the Test A.

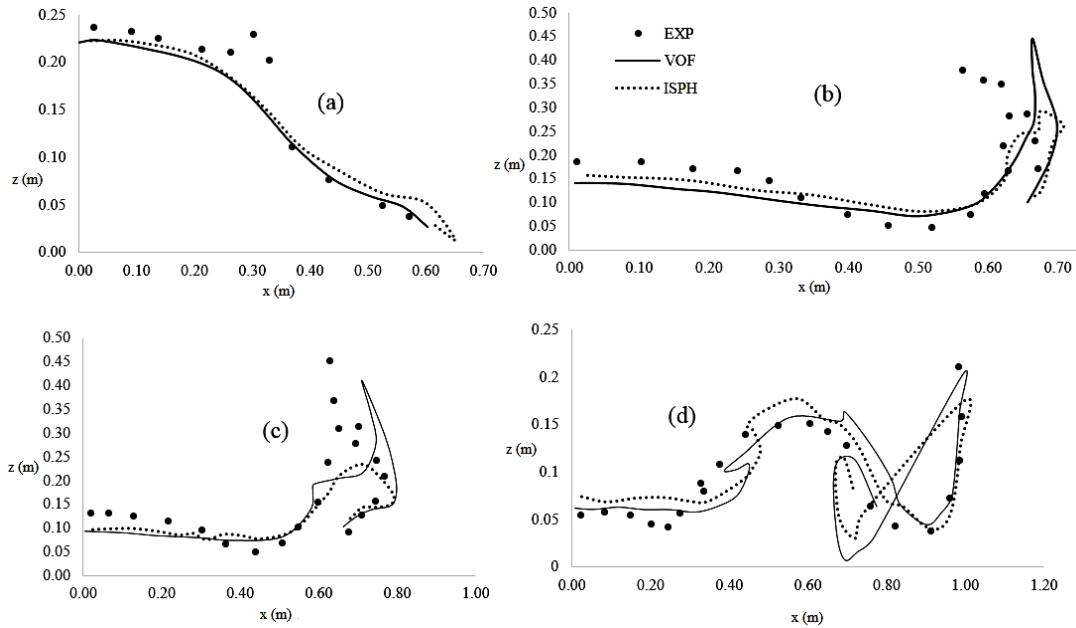


Fig. 9. Comparison between numerical results (ISPH; dotted, and FV-VOF: solid line) and experimental observations in the Test A; the experimental digitized free-surface position is shown by the circles; a) 0.2 s, b) 0.4 s, c) 0.6 s, d) 0.8 s.

Table 1. MAE of numerical modeling results versus experimental observations for the position of the wave height in the Test A.

Time(s)	MAE of FV-VOF	MAE of ISPH
0.2	0.0098	0.0113
0.4	0.0287	0.0261
0.6	0.0211	0.0199
0.8	0.0098	0.0157

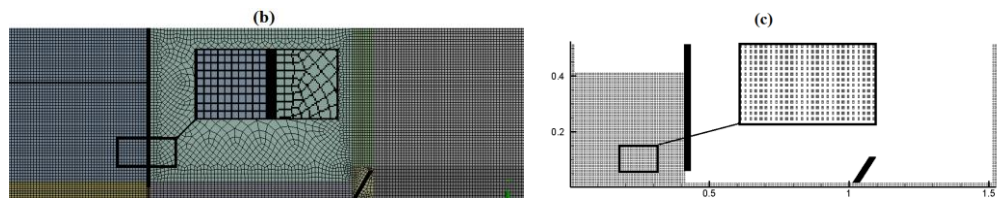


Fig. 10. b) schematic view of FV-VOF quadrilateral meshes, c) schematic view of initial layout of particles in the ISPH method.

and it is suitable factor for examine the accuracy of observed and calculated data.

$$MAE = \frac{1}{N} \sum_{i=1}^N |numerical - exp| \quad (6)$$

MAEs of 0.06 m, and 0.07 m are obtained for the simulated wavefront position using FV-VOF model, and ISPH model, respectively. This indicates that two models yield good results that are accurate enough. Table 1 represents the MAE of variation of free-surface elevation between the numerical and

experimental data at different times. Results show that two models approximately have same accuracy; however, in some times FV-VOF model is superior to ISPH Model, and vice versa. In general, both models have acceptable accuracy in simulating this test.

4.2.2. Numerical Modeling of Abrupt Wave Impact with an Inclined Obstacle

The schematic representation of the geometry of the wave flume as well as the discrete computational domains of FV-VOF and ISPH models are shown in Fig. 10. The value of the numerical simulation parameters are presented in Table 2.

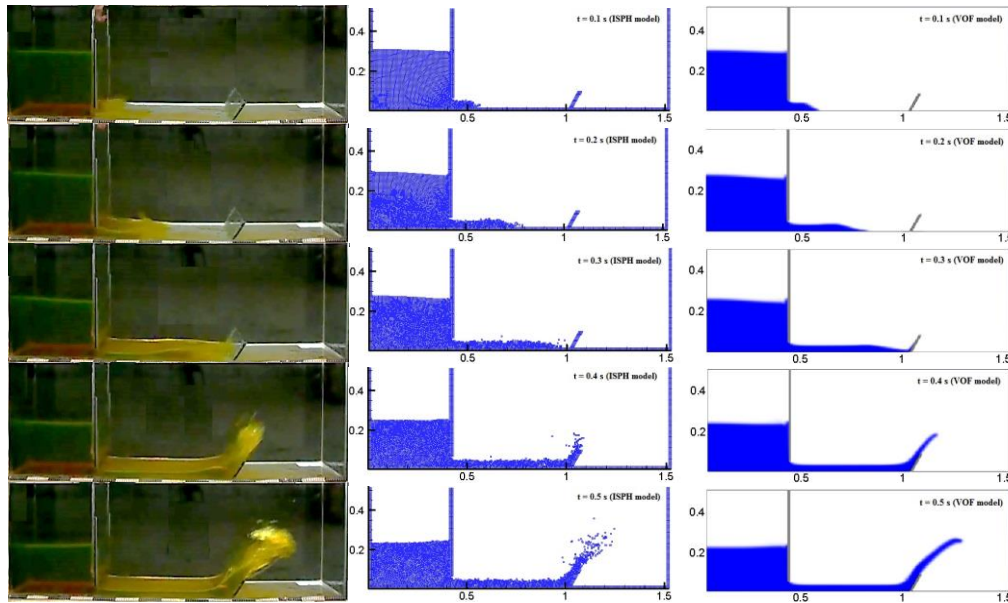


Fig. 11. Snapshots of calculated results (FV-VOF on the right and ISPH in the middle) and laboratory photographs (on the left), $H=0.3$ m, $L=0.4$ m, at times 0.1, 0.2, 0.3, 0.4, and 0.5 s.

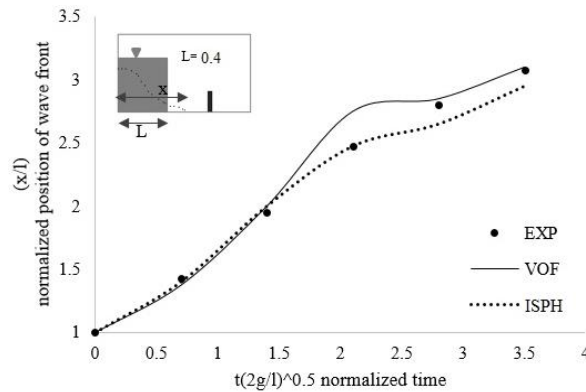


Fig. 12. Experimental versus numerical normalized diagram of wave front position for the Test B.

Table 2 General characteristics of applied meshes and time-steps for the Test B

Numerical model	Time steps (s)	Number of particles	Number of elements
FV-VOF	0.001-0.5	-	9818
ISPH	0.0004	5898	-

The numerical results of both FV-VOF and ISPH models are compared with experimental observations in Fig. 11. For a better understanding and more accurate analysis of results, the computed and measured wave front positions as a function of normalized time is shown in Fig. 12, and the comparison between computed and measured free surface profiles is given in Fig. 13. Figure 13 shows good agreement between numerical and experimental results.

In this test, MAE of simulated wavefront position using FV-VOF model and ISPH model has been obtained 0.07 m, and 0.05 m, respectively.

Therefore, the ISPH model has lower error in this step. Table 3 represents the MAE of variation of free-surface elevation between the numerical and experimental data at different times. In this test, evaluation of Table 3 and diagrams show that the accuracy of the ISPH model was higher than that of the FV-VOF model.

To analyze the performance of the numerical methods, comparisons between the computational times in the two cases are presented in table 4. According to the tabulated results, the computational time of modeling by ISPH (initial distance between the particles: 0.006 m) was less than the time of modeling by FV-VOF. Since the computation time is an important parameter in numerical modeling processes, it can be concluded that the ISPH model can be considered as the more efficient model in this study. However, it should be noted that if the initial distance between the particles in the SPH method were considered less than 0.006 m, the computation time would increase significantly.

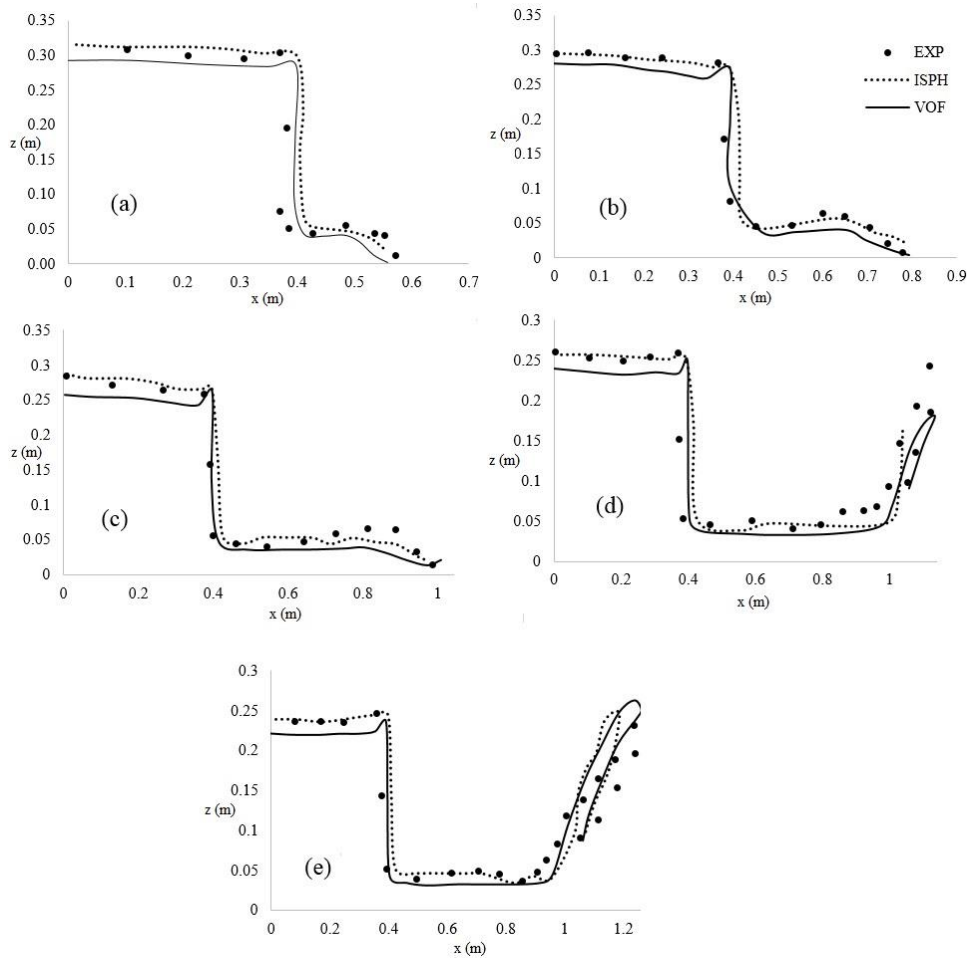


Fig. 13. Comparison between numerical results (ISPH: dotted, and FV-VOF: solid line) and experimental observations in the Test B; the experimental digitized free-surface position is shown by the circles; a) 0.1 s, b) 0.2 s, c) 0.3 s, d) 0.4 s, e) 0.5 s.

Table 3 MAE of numerical modeling results versus experimental observations for the position of the wave height in the Test B

Time(s)	MAE of FV-VOF	MAE of ISPH
0.1	0.0153	0.0080
0.2	0.0150	0.0010
0.3	0.0171	0.0073
0.4	0.0178	0.0043
0.5	0.0188	0.0075

Table 4 Computational time to solve the simulated problems using a dual core (3.07 GHz – 3.06 GHz) CPU

Experimental test	Time duration of numerical modeling (hr)	
	ISPH model	FV-VOF model
Test A	4.81	10.12
Test B	7.58	16.78

Table 5 Comparison of averaged velocity of position of the wave front to solve the simulated problems using FV-VOF and ISPH models and the experimental model

velocity of position of the wave front (m/s)	ISPH model	FV-VOF mode	experimental
Test A	1.84	1.89	1.78
Test B	3.7	3.58	3.63

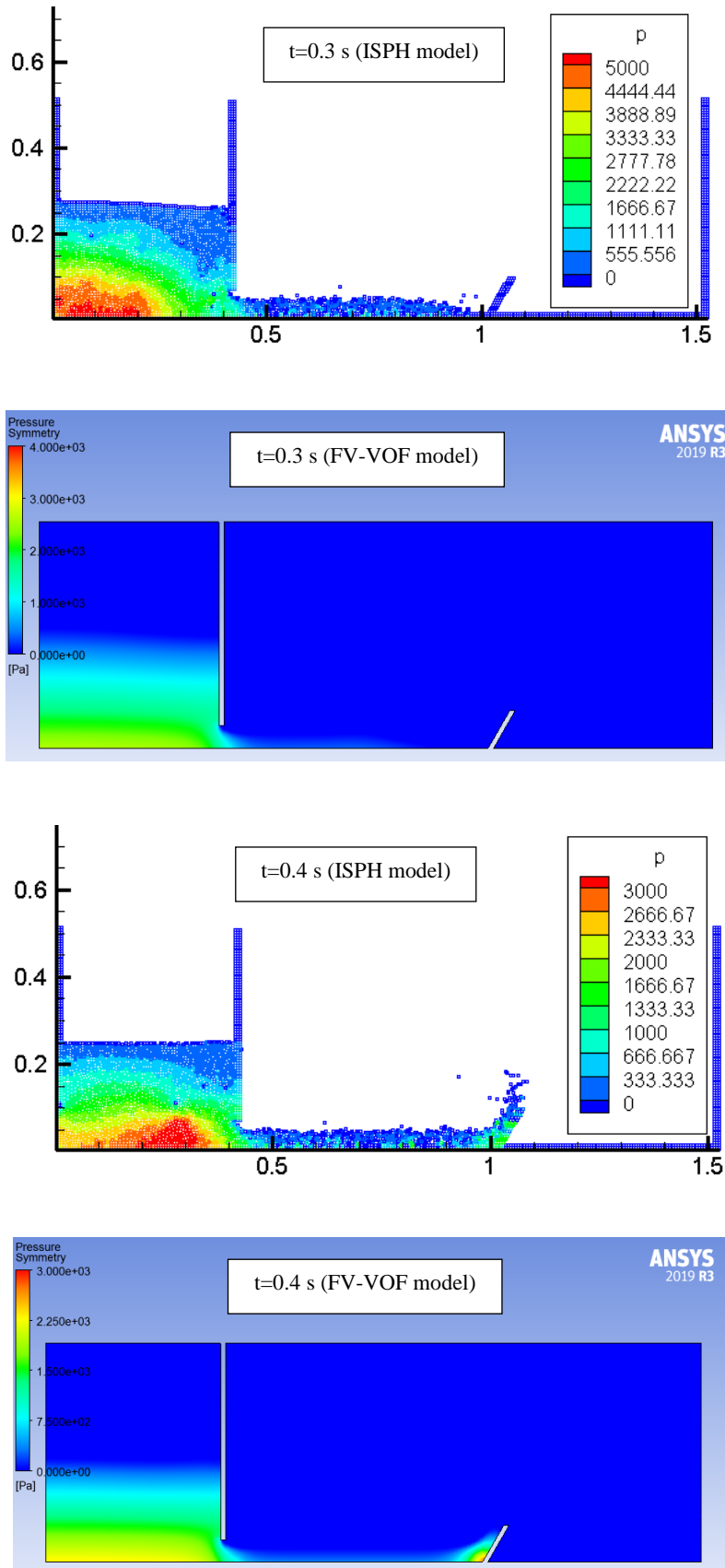


Fig. 14. Pressure field of abrupt wave impact with an inclined obstacle problem computed by ISPH and FV-VOF models (Unit of pressure is Pascal).

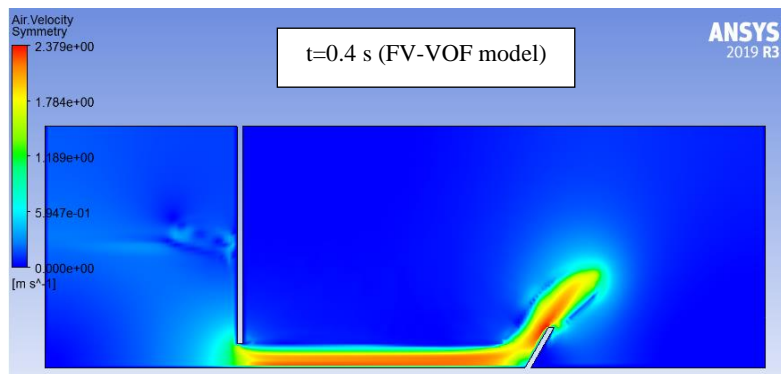
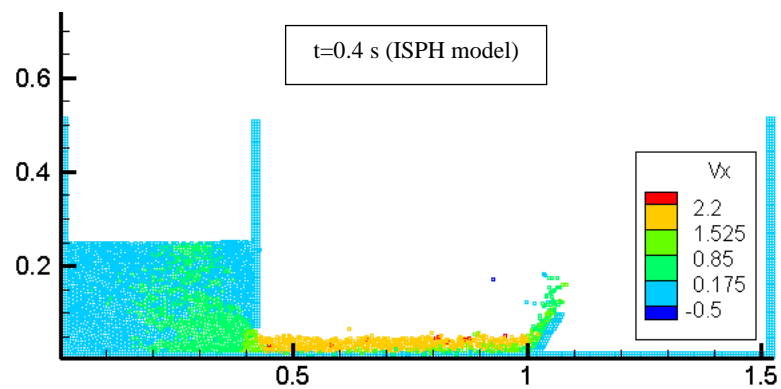
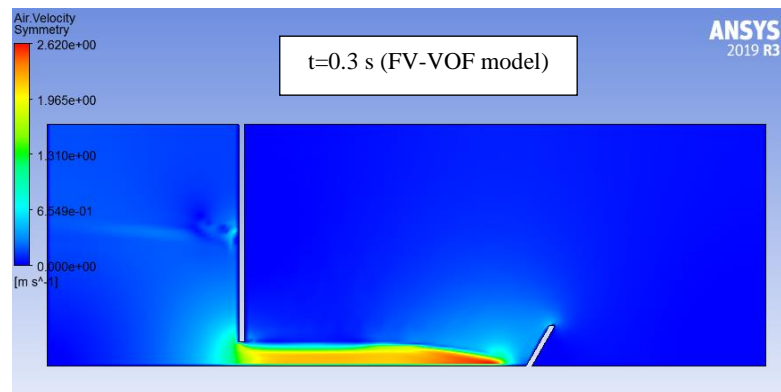
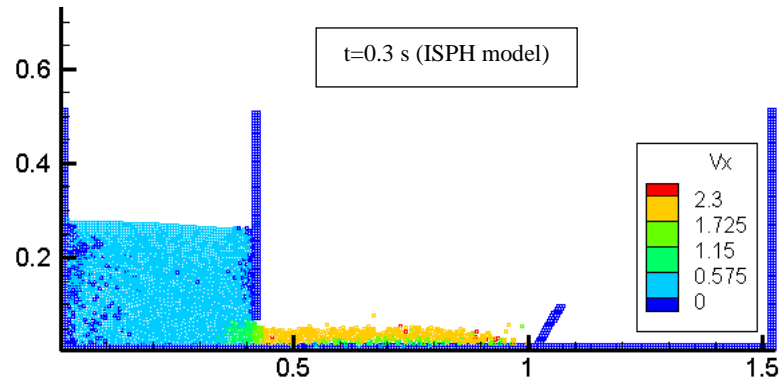


Fig. 15. Horizontal velocity field of abrupt wave impact with an inclined obstacle problem computed by ISPH and FV-VOF models (Unit of velocity is m/s).

Table 5 compares the computed averaged X-component velocity with the experimental measurements in the experimental tests. This comparison shows the good agreement between the results of numerical models (FV-VOF and ISPH) and the experimental results. Figure 14 shows the computational pressure field by numerical models at two different times. As can be seen from this figure, the pressure calculated by numerical models has a relatively smooth distribution without large noises. However, some small fluctuation in the pressure field is visible in the ISPH results. This can be due the ISPH unphysical fluctuations. Overall, this relatively good calculation of the pressure field by the models has led to the simulation with appropriate accuracy of the free flow surface profile and other hydraulic properties of the flow field. Furthermore, Fig. 15 shows the horizontal velocity field calculated by two numerical models. This figure shows the approximate similarity of the velocity field calculated by the models. These sample problems show the ability of the proposed models to simulate the flow features of fluid-structure interaction problems accurately.

5. CONCLUSION

The present study has investigated the interaction of the abrupt wave with the solid obstacles. This issue was studied through experimental and numerical modeling. Two experiments including abrupt wave impact with the vertical and inclined obstacle have been performed in the Water Engineering Laboratory of the Shahid Bahonar University of Kerman. Furthermore, the ability of two famous numerical models, including ISPH and FV-VOF, has been studied in reproducing the impact of an abrupt wave with rigid obstacles. The performance of these models has been assessed by comparing the numerical predictions of free surface profiles with the experimental data. The results demonstrate that both numerical models simulate the free surface profile with suitable accuracy. The results of the present paper can be used for the selection of the suitable model for the numerical study of the interaction of an abrupt wave with obstacles.

REFERENCES

- Albano, R., A. Sole, D. Mirauda and J. Adamowski (2016). Modelling large floating bodies in urban area flash-floods via a Smoothed Particle Hydrodynamics model. *Journal of Hydrology* 541, 344-358.
- Aureli, F., S. Dazzi, A. Maranzoni, P. Mignosa and R. Vacondio (2015). Experimental and numerical evaluation of the force due to the impact of a dam-break wave on a structure. *Advances in Water Resources* 76, 29-42.
- Bukreev, V. I. (2009). Force action of discontinuous waves on a vertical wall. *Journal of applied mechanics and technical physics* 50(2), 278-283.
- Canelas, R. B., A. J. Crespo, J. M. Domínguez, R. M. Ferreira and M. Gómez-Gesteira (2016). SPH-DCDEM model for arbitrary geometries in free surface solid-fluid flows. *Computer Physics Communications* 202, 131-140.
- Canelas, R. B., M. Brito, O. G. Feal, J. M. Domínguez and A. J. C. Crespo (2018). Extending DualSPHysics with a Differential Variational Inequality: modeling fluid-mechanism interaction. *Applied Ocean Research* 76, 88-97.
- Chang, T. J., H. M. Kao, K. H. Chang and M. H. Hsu (2011). Numerical simulation of shallow-water dam break flows in open channels using smoothed particle hydrodynamics. *Journal of Hydrology* 408(1-2), 78-90.
- Chen, R., S. Shao, X. Liu and X. Zhou (2015). Applications of shallow water SPH model in mountainous rivers. *Journal of Applied Fluid Mechanics* 8(4), 863-870.
- Crespo, A. J., M. Gómez-Gesteira and R. A. Dalrymple (2008). Modeling dam break behavior over a wet bed by a SPH technique. *Journal of Waterway, Port, Coastal, and Ocean Engineering* 134(6), 313-320.
- Hosseinkhani, M. R., P. Omidvar, S. Allahyaribeik and M. T. Azad (2020). Simulation of Waves on Boom and Oil Plume Rising using Smoothed Particle Hydrodynamics. *Journal of Applied Fluid Mechanics* 13(1), 39-54.
- Hui Pu, J., S. Shao, Y. Huang and K. Hussain (2013). Evaluations of SWEs and SPH numerical modelling techniques for dam break flows. *Engineering Applications of Computational Fluid Mechanics* 7(4), 544-563.
- Khayyer, A., H. Gotoh, Y. Shimizu, K. Gotoh, H. Falahaty and S. Shao (2018). Development of a projection-based SPH method for numerical wave flume with porous media of variable porosity. *Coastal Engineering* 140, 1-22.
- Kheirkhahan, M., P. Omidvar and K. H. Hosseini (2020). Effective Pressure for Two Phase Water-Sediment Models using SPH Method. *Journal of Applied Fluid Mechanics* 13(4).
- López, D., T. Ramos, P. Sánchez, R. Marivela, R. Díaz, J. J. Rebollo, F. R. Andres, V. Cuellar, M. De Blas and J. L. Garcia. (2018). Smoothed Particle Hydrodynamics Method for Three-Dimensional Open Channel Flow Simulations. *Journal of Applied Fluid Mechanics* 11(6), 1599-1611.
- Marrone, S., M. A. G. D. Antuono, A. Colagrossi, G. Colicchio, D. Le Touzé and G. Graziani, (2011). δ -SPH model for simulating violent impact flows. *Computer Methods in Applied Mechanics and Engineering* 200(13-16), 1526-1542.
- Memarzadeh, R. and K. Hejazi (2012). ISPH numerical modeling of nonlinear wave run-up on steep slopes. *Journal of the Persian Gulf (Marine Sciences)* 3(10), 17-26.

- Memarzadeh, R., G. Barani and M. Ghaeini-Hessaroeyeh (2018). Application of a weakly compressible smoothed particle hydrodynamics multi-phase model to non-cohesive embankment breaching due to flow overtopping. *Frontiers of Structural and Civil Engineering* 12(3), 412-424.
- Monaghan, J. J. (2000). SPH without a tensile instability. *Journal of computational physics* 159(2), 290-311.
- Ozmen-Cagatay, H., S. Kocaman and H. Guze (2014). Investigation of dam-break flood waves in a dry channel with a hump. *Journal of Hydro-Environment Research* 8(3), 304-315.
- Shao, S. (2010). Incompressible SPH flow model for wave interactions with porous media. *Coastal Engineering* 57(3), 304-316.
- Shao, S. and E. Y. Lo (2003). Incompressible SPH method for simulating Newtonian and non-Newtonian flows with a free surface. *Advances in Water Resources* 26(7), 787-800.
- Soares-Frazão, S. and Y. Zech (2007). Experimental study of dam-break flow against an isolated obstacle. *Journal of Hydraulic Research* 45(sup1), 27-36.
- Tang, Z. Y., Y. L. Zhang and D. C. Wan (2016). Numerical simulation of 3-D free surface flows by overlapping MPS. *Journal of hydrodynamics Ser. B*, 28(2), 306-312.
- Versteeg, H. K. and W. Malalasekera (2007). An introduction to computational fluid dynamics: the finite volume method. Pearson education.
- Xu, X., J. Ouyang, B. Yang and Z. Liu (2013). SPH simulations of three-dimensional non-Newtonian free surface flows. *Computer Methods in Applied Mechanics and Engineering* 256, 101-116.
- Zhang, N., X. Zheng, Q. Ma, W. Duan, A. Khayyer, X. Lv and S. Shao (2018). A hybrid stabilization technique for simulating water wave-Structure interaction by incompressible Smoothed Particle Hydrodynamics (ISPH) method. *Journal of hydro-Environment Research* 18, 77-94.